Quantitative Analysis of Microstructural Constituents in Welded Transformation-Induced-Plasticity Steels

M. AMIRTHALINGAM, M.J.M. HERMANS, L. ZHAO, and I.M. RICHARDSON

A quantitative analysis of retained austenite and nonmetallic inclusions in gas tungsten arc (GTA)–welded aluminum-containing transformation-induced-plasticity (TRIP) steels is presented. The amount of retained austenite in the heat-affected and fusion zones of welded aluminum-containing TRIP steel with different base metal austenite fractions has been measured by magnetic saturation measurements, to study the effect of weld thermal cycles on the stabilization of austenite. It is found that for base metals containing 3 to 14 pct of austenite, 4 to 13 pct of austenite is found in the heat-affected zones and 6 to 10 pct in the fusion zones. The decomposition kinetics of retained austenite in the base metal and welded samples was also studied by thermomagnetic measurements. The decomposition kinetics of the austenite in the fusion zone is found to be slower compared to that in the base metal. Thermomagnetic measurements indicated the formation of ferromagnetic ε carbides above 290 °C and paramagnetic $\eta(\varepsilon')$ transient iron carbides at approximately 400 °C due to the decomposition of austenite during heating.

DOI: 10.1007/s11661-009-0117-6

I. INTRODUCTION

TRANSFORMATION-INDUCED-PLASTICITY (TRIP) steels are one class of advanced high-strength steels that offer a combination of high strength (tensile strengths of 500 to 1000 MPa), high formability (uniform elongation 20 to 40 pct), and high dynamic energy absorption during high-strain-rate crash deformation (350 MJ/m^3 at 1000 s^{-1}). The use of high-strength thinner-gage TRIP steels reduces the weight of the automobiles and thus can potentially reduce fuel consumption.[1] Moreover, the higher dynamic energy absorption during a crash improves the passenger safety and the crashworthiness of the vehicle. These combinations of properties are achieved mainly by the deformation-induced transformation of austenite to martensite. Thus, TRIP steels ought to have suitable alloying elements and heat treatment to develop multiphase microstructures with a mixture of ferrite, bainite, and austenite retained at room temperature. Unfortunately, the commercial applicability of TRIP steels is limited by their poor weldability, which is due to the higher alloying content. The thermal cycle of a welding process destroys the carefully designed microstructure, which results in inferior mechanical properties of the weld. A previous microstructural analysis during the welding of silicon and aluminum-based TRIP steels showed the formation of complex inclusions in the fusion zones of high-Si and high-Al TRIP steels. These inclusions were found to be comprised of several substructural features with different compositions. The formation of allotriomorphic ferrite was found at the fusions line and the grain boundaries of high-Al steel welds. The partitioning of aluminum to the solidified δ ferrite led to the stabilization of ferrite at the fusion lines and at columnar grain boundaries.[2,3] In TRIP steel welds, the formation of hard intermetallic inclusions in the fusion zones and the presence of soft ferritic grains at the fusion boundaries invariably change the partitioning behavior of alloying elements during the phase transformations and affect the stabilization behavior of retained austenite across the weld zone. Thus, in order to improve the weldability of these steels, it is necessary to understand the influence of weld thermal cycles on the microstructural evolution during welding, with a special emphasis on the retained austenite distribution in the weld microstructure.

The magnetic saturation technique has developed into a reliable method for accurately quantifying austenite contents in steels. It measures the bulk magnetic properties of the specimen and, in comparison to other experimental techniques, is easy to use without complex sample preparation.[4] In this method, the saturation magnetizations of steel samples with and without austenite are measured from the magnetization curves (magnetic flux density as a function of mass magnetization). Ferrite, martensite, and cementite are ferromagnetic below their Curie temperature (T_c) in steels, while austenite and nonmetallic inclusions are paramagnetic (for pure ferrite, T_c is 770 °C and for cementite, T_c is 210 °C). Thus, the difference in the saturation

M. AMIRTHALINGAM, Ph.D. Researcher, and L. ZHAO, Research Fellow, are with the Materials Innovation Institute, 2628 CD, Delft, The Netherlands. Contact e-mail: a.murugaiyan@tudelft.nl M.J.M. HERMANS, Assistant Professor, and I.M. RICHARDSON, Professor and Head, are with Joining and Mechanical Behaviour, Department of Material Science and Engineering, Delft University of Technology, 2628 CD, Delft, The Netherlands.

Manuscript submitted June 8, 2009.
Article published online December 2, 2009

magnetization is directly proportional to the amount of paramagnetic phases in the steel samples.[4,5]

In this work, attempts are made to estimate the austenite and nonmetallic inclusion content in the heat-affected and fusion zones of gas tungsten arc (GTA)–welded aluminum-based TRIP steels using the magnetic saturation method. Bead-on-plate welding was performed on TRIP steel plates with four different heat-treatment conditions, which created initial austenite contents varying from 3 to 14 pct. Magnetic measurements were then carried out on samples taken from the weld regions covering the base metal, heat-affected, and fusion zones. The magnetic saturation values were also measured while tempering the austenite-containing base metal samples and the fusion zone samples at 600 °C, in order to study the decomposition kinetics of austenite in welded TRIP steels.

II. EXPERIMENTAL PROCEDURE

A commercially available 1.25-mm-thick aluminum-containing TRIP steel in a cold-rolled condition was used in this study. The total content of the alloying elements was 3.3 wt pct, of which 1.1 pct was aluminum (Table I). This high aluminum content ensured the suppression of cementite formation, subsequently enriching austenite with carbon so that it is stabilized at room temperature. Sample plates for GTA welding experiments with a length of 250 mm and a width of 100 mm were cut from the steel plates and subjected to specific TRIP heat-treatment cycles using salt baths. Two intercritical ($\alpha + \gamma$) annealing temperatures (IATs) and isothermal bainitic holding temperatures were used to generate base microstructures with four different austenite contents (Figure 1). The notations of the heat treatments mentioned in Figure 1 are used throughout this article. Bead-on-plate welding was performed on

Table I. Composition of Steel under Investigation

Elements	C	Mn	Si	Cr	Al	S	P
Weight percent	0.19	1.63	0.35	0.019	1.1	—	0.089

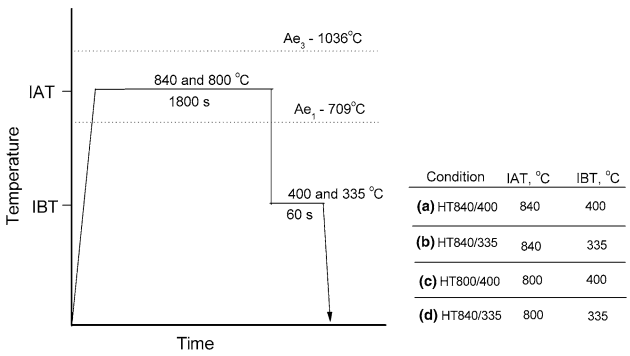

Fig. 1—Schematic illustration of the heat-treatment cycle applied to the base metals, with IAT and IBT temperature. (The inset table shows four different heat-treatment conditions.)

these heat-treated plates using automated GTA welding equipment; the welding parameters used are shown in Table II.

The GTA welding was carried out using a Migatronic Commander 400 AC/DC power source (Migatronic Automation A/S, Aabybro, Denmark). An automatic voltage-control algorithm was used to keep the voltage constant during welding. The conditions resulted in full-penetration welds with a top width of approximately 5 mm. During welding, the samples were clamped to a steel backing plate with a 20-mm-wide central groove for purging argon backing gas. At 125 mm from the starting edge of the samples, the backing plate has a 20-mm-wide groove perpendicular to the welding direction, to allow thermocouple measurements to be made on the underside of the samples. *In-situ* temperature measurements were performed during bead-on-plate welding using 0.25-mm-diameter K-type thermocouples, which were discharge welded to the lower surface of the plates on a line perpendicular to the weld seam, starting 2.5 mm from either side of the weld centerline, with interdistances of approximately 3 mm between the measurement points. After welding, the plates were cross sectioned in the transverse direction for metallographic analysis. For optical microscopy analysis, two etching procedures were followed to clearly delineate the microstructural constituents present in the weldments. In the first procedure, samples were etched with 4 pct nital solution for 5 seconds for the overview of the weld microstructure. A second etching method was used to examine the presence of retained austenite in the microstructure. In this method, samples were etched for 15 seconds with 4 pct Picral, followed by 30 seconds etching in 1 pct sodium metabisulfite solution in water. This etching procedure changes the colors of the retained austenite/martensite into bright whitish blue, bainite into brown, and allotriomorphic ferrite into a tan color.[6] The samples were subsequently analyzed using optical microscopy.

Cylindrical samples 1.25 mm in diameter were cut by means of electrodischarge machining from the welded plates at five different places in and around the weld zone for the magnetic saturation measurements. Figure 2 schematically shows the positions from which samples were taken. Three samples along the length of the weld were taken at different transverse locations to ensure repeatability, and measurements were averaged to improve the statistical relevance. Note that the left and right sides of the weld centerline are treated separately for this purpose. The magnetization measurements were

Table II. Welding Parameters

Electrode	W + 2 wt pct ThO_2
Electrode diameter	2.4 mm
Electrode tip angle	60 deg
Arc length	3 mm
Voltage	10.7 V
Current	65 A
Welding speed	7 mm/s
Shielding gas	Ar, 10 L/min
Shielding cup diameter	8 mm

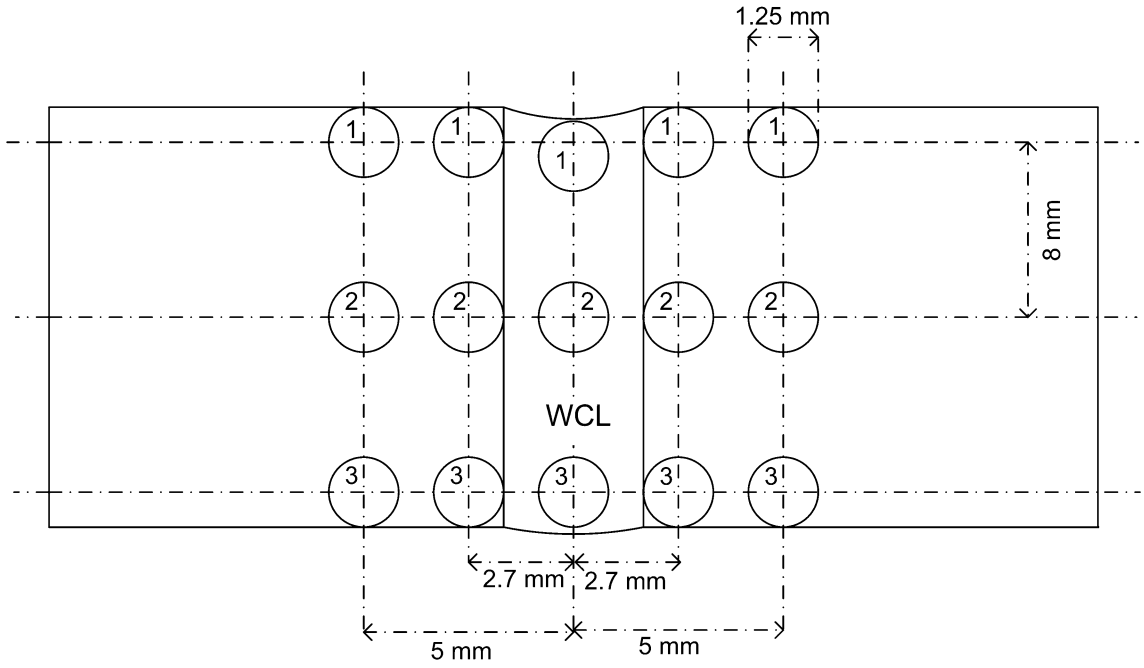

Fig. 2—Schematic representation of various places from which samples were cut from the welded plate. Here, WCL is the weld centerline. Samples representing the heat-affected zone were taken at 2.7 and 5 mm from the weld centerline. (Note: Measurements from samples 1 through 3 at each transverse location were averaged.)

performed in a LakeShore 7307* vibration sample magnetometer and were carried out by applying magnetic fields starting from 2 T to zero and then to –2 T with a step size of 0.05 T. This decreasing field measurement was made to ensure a well-defined field history for the magnetization. Throughout the measurements, stability and accuracy were checked by periodic calibration of the equipment using a nickel-standard sample with a sensitivity of 1×10^{-11} Am^2. A high-temperature oven (model LakeShore 73034**) attached to the magnetometer was used for the thermomagnetic measurements. The saturation magnetization (M_s) of the steel samples was calculated from the mass magnetization as a function of the magnetic field curves. The accuracy in the measurement of the saturation magnetization of the TRIP steel samples was found to be ± 0.01 Am^2/kg.[7] A detailed description of these calculations can be found elsewhere.[4,8]

*LakeShore 7307 is a trademark of LakeShore Cryotronics, Inc, Westerville, OH.

**LakeShore 73034 is a trademark of LakeShore Cryotronics, Inc, Westerville, OH.

III. RESULTS

A. *Characteristics of Base Metals*

Optical microscopy analysis clearly indicates the presence of austenite after the heat treatments (Figure 3). The size of austenite grains in these microstructures are found to vary from 2 to 5 μm. The austenite content appears to be higher in the case of condition HT800/400, which is also found to contain coarser austenitic grains compared with the other conditions. In order to measure the amount of austenite present in the samples, one of the base metal samples was heated to 600 °C and cooled to room temperature at a rate of 0.03 °C s^{-1}, to transform the austenite present in the sample to a ferrite and cementite mixture.[9] The saturation magnetization of the sample without austenite ($M_s(f)$) was measured at room temperature and the mass fraction of austenite f_γ present in the sample was calculated using the relationship

$$f_\gamma = 1 - \beta \frac{M_s(c)}{M_s(f)} \quad [1]$$

where $M_s(c)$ is the saturation magnetization of austenite-containing samples (Am^2/kg) and the coefficient β is 0.99,[4] which takes into account the effect of cementite on the saturation magnetization. The magnetization curves for the heat-treated base metal samples and the sample without austenite are shown in Figure 4, in which the approach to the saturation magnetization clearly differs in all cases. The saturation magnetization of the sample without austenite ($M_s(f)$) was found to be 216.4 Am^2/kg. Table III shows the saturation magnetization values of heat-treated samples and their corresponding austenite contents calculated using Eq. [1]. The heat-treatment condition HT800/400 yielded a base metal microstructure with a higher amount of austenite (14.0 pct) compared with other heat-treatment conditions. It should also be noted that conditions with higher isothermal bainitic transformation

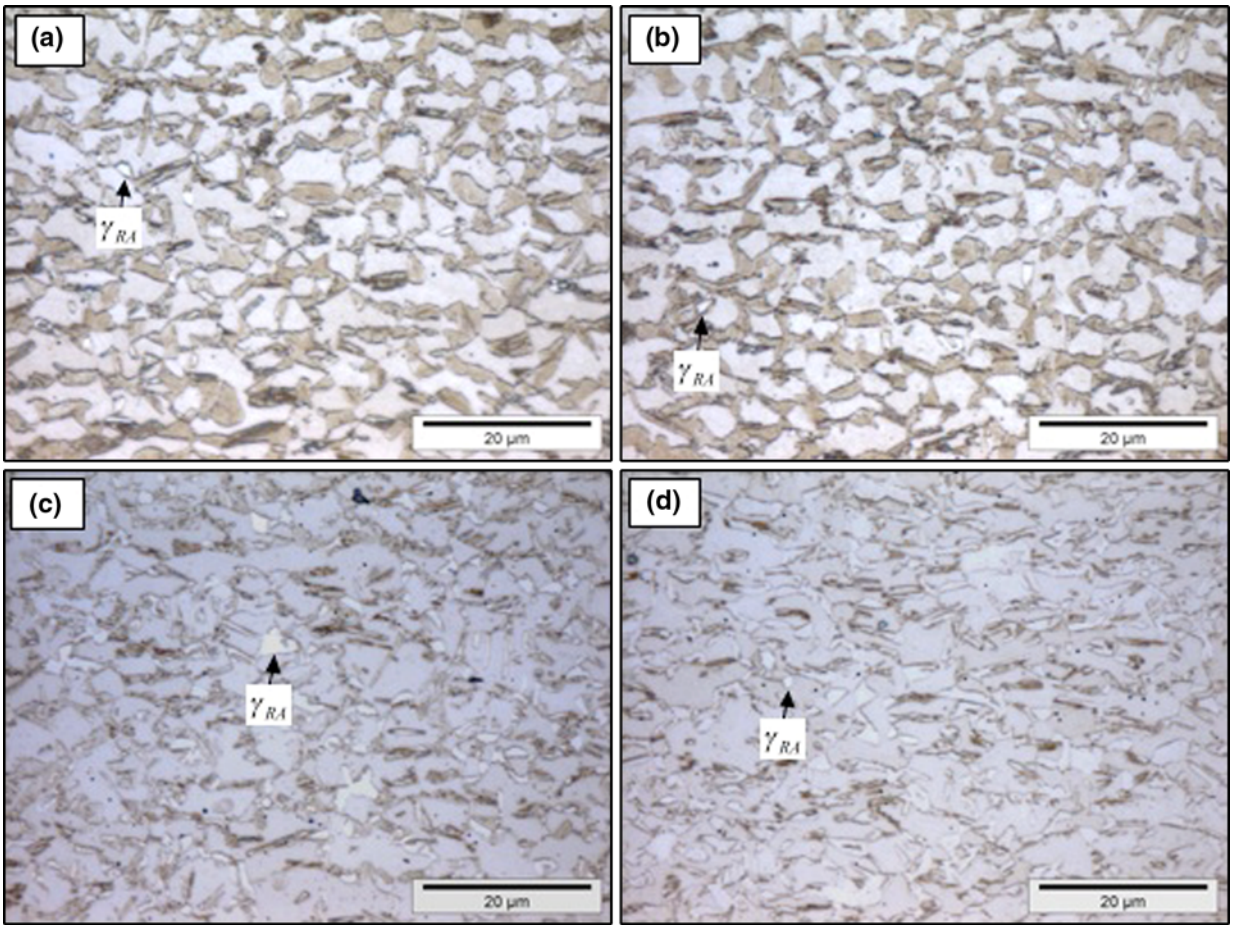

Fig. 3—Optical micrographs of base metals after the four heat treatments ((a) through (d) in Table III) showing the presence of austenite (bright) along with ferrite (matrix) and bainite (dark).

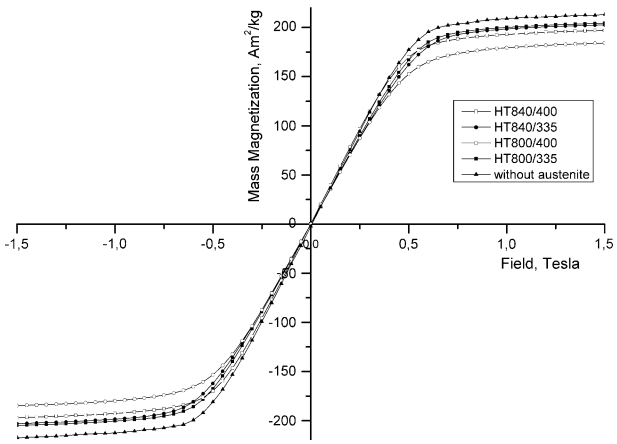

Fig. 4—Magnetization of heat-treated base metals and sample without austenite as a function of the magnetic field. (Saturation magnetization values (M_s) were measured from these curves with an accuracy of ±0.01 Am^2/kg.)

(IBT) temperatures (in this case, HT840/400 and HT800/400) generated more austenite in the microstructures.

Table III. Saturation Magnetization and Austenite Contents in Heat-Treated Base Metals (Accuracy in Retained Austenite Measurements is ± 0.2 Percent)

Heat-Treatment Condition	Saturation Magnetization (Am^2/kg)	Austenite (Pct)
(a) HT840/400	197.1	8.9
(b) HT840/335	208.7	3.6
(c) HT800/400	186.2	14.0
(d) HT800/335	207.2	4.3

B. *Characteristics of Welded TRIP Steel Plates*

The temperature cycles at specific locations across the width of the steel plate (condition HT840/400) during welding is shown in Figure 5. The width of the fusion zone was 5 mm. The maximum temperature at a point 2.6 mm from the weld centerline was 980 °C, where maximum heating and cooling rates (550 °C/s to 200 °C/s) were also observed. The temperature profiles remained the same during welding of the other three heat-treated plates, because plates of the same thickness were welded with the same parameters in all cases. The optical microscopy analysis showed that the fusion and heat-affected zones of GTA-welded TRIP steels contained

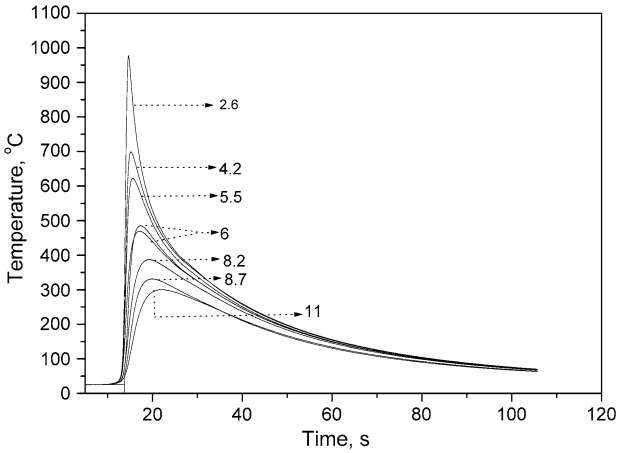

Fig. 5—Temperature profile during GTA welding of TRIP steel plate (HT840/400). The numbers indicate the distance of the measurement points from the weld centerline (mm).

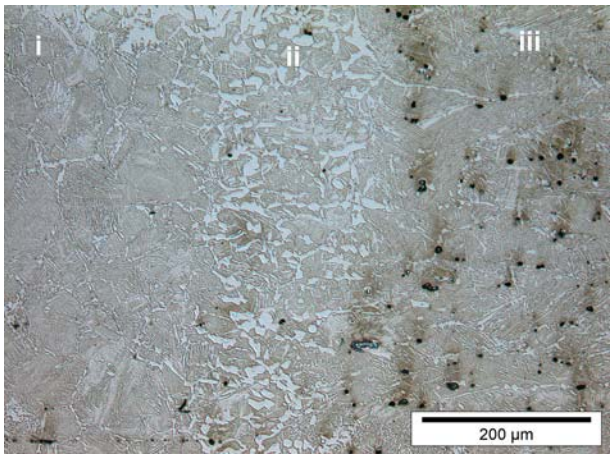

Fig. 6—Optical micrograph of a TRIP steel (HT840/400) weld showing (i) coarse-grained heat-affected zone with grain boundary ferrite, (ii) ferritic fusion line, and (iii) inclusion-containing fusion zone.

primarily a martensitic microstructure, which can be seen in Figure 6, in which a microstructure of a welded TRIP steel plate (condition HT840/400) is shown. In addition, the fusion zones of all welded steels show the presence of inclusions, mainly decorating the grain boundaries, and a zone of soft allotriomorphic ferritic grains was found along the fusion lines. Although the optical microscopy analysis did not delineate the presence of austenite in the fusion and heat-affected zones, the magnetization behavior of samples from the heat-affected and fusion zones showed differences in the saturation magnetizations, which indicated variations in the amount of paramagnetic phases, in this case, austenite and nonmetallic inclusions. This is reflected in Figure 7, in which the magnetization behavior of the samples taken from the heat-affected and fusion zones of welded plates is shown.

Quantitative estimations of austenite contents in the heat-affected zones were carried out using Eq. [1]. In the fusion zones, nonmetallic inclusions were found during optical microscopy analysis and measurements of

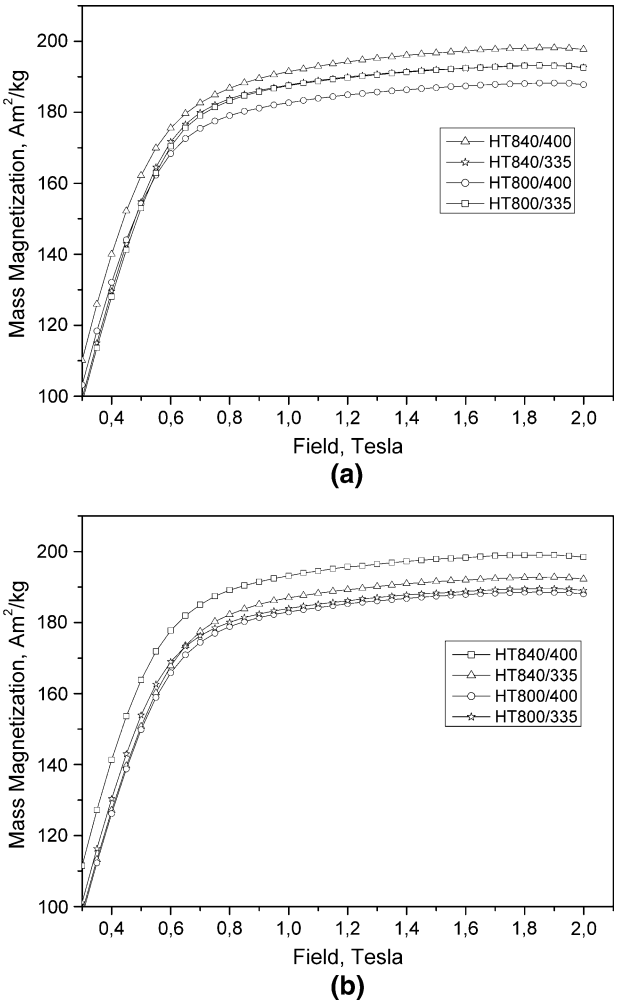

Fig. 7—Magnetization behavior of samples from (*a*) heat-affected and (*b*) fusion zones of TRIP steel welds. (Saturation magnetization values (M_s) are measured from these curves with an accuracy of ±0.01 Am^2/kg.)

retained austenite contents in fusion zones were corrected for the amount of nonmetallic inclusions. In order to calculate the nonmetallic inclusion contents, the saturation magnetization of fusion zone samples without austenite ($M_s(i)$) was measured after transforming the austenite present in the sample to ferromagnetic ferrite and cementite by tempering at 600 °C. The nonmetallic inclusions present in the fusion zone remain untransformed during this tempering process.[10] The mass fraction of inclusions (f_i) was calculated by comparing the saturation magnetization of a fusion zone sample without austenite ($M_s(i)$) to the base metal sample without austenite ($M_s(f)$) using the relationship:

$$f_i = 1 - \beta \frac{M_s(i)}{M_s(f)} \qquad [2]$$

The average saturation magnetization of the fusion zone samples without austenite but with inclusions ($M_s(i)$) was found to be 210.9 Am^2/kg, compared to 216.4 Am^2/kg for the base metal sample without austenite. Thus, the average inclusion content in the fusion zones of welded TRIP steels was 2.6 pct. The final austenite

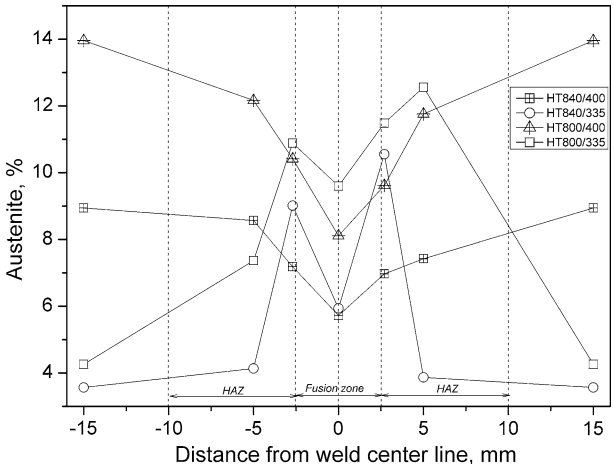

Fig. 8—Retained austenite variation across the width of welded TRIP steel plates (accuracy in retained austenite measurement is ±0.2 pct).

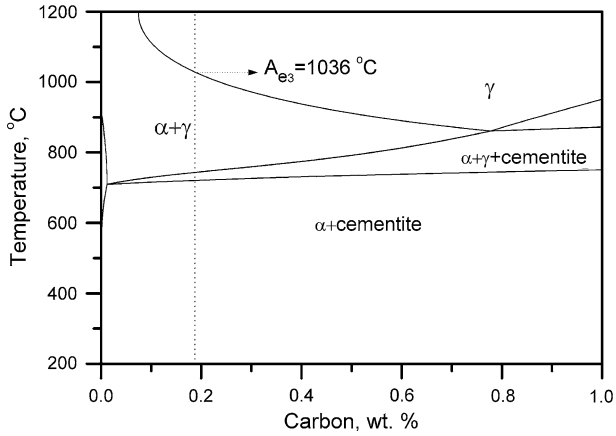

Fig. 9—Pseudobinary diagram of the steel under investigation (Table I, for the composition), indicating that the A_{e_3} temperature is 1036 °C.

contents in the fusion zones were then calculated using Eq. [1] and subtracting the inclusion contents. The samples in the heat-affected zones were not corrected for inclusions, because the presence of inclusions was not confirmed by optical microscopy.

The variation in the austenite contents in the welded TRIP steel plates are shown in Figure 8, after correcting the nonmetallic inclusion contents in the fusion zones. It should be noted that the magnetic measurements were carried out on 1.25-mm-diameter samples and thus represent averages over the volume of the sample. In Figure 8, the average austenite contents of the samples are plotted against the distance of the center of the samples from the weld centerline. It is interesting to note that approximately 4.1 to 12.7 pct of the austenite is found in the heat-affected zones and 5.7 to 9.6 pct in the fusion zones, despite the fact that both the fusion and heat-affected zones undergo a weld thermal cycle with heating and cooling rates varying from 550 °C/s to 200 °C/s.

C. *Decomposition Behavior of Austenite*

Thermomagnetic measurements were carried out to investigate the thermal stability of retained austenite in the TRIP steel base metal. During welding, in the region directly alongside the fusion lines (in the present case, approximately 2.5 mm from the weld centerline), the peak temperature could reach above A_{C_3} and, depending on the location, steel may become fully austenitic. The pseudobinary diagram (Figure 9) indicates that the steel becomes fully austenitic after heating above 1036 °C (A_{e_3} temperature of this steel). The peak temperature reached during welding decreases with the distance from the weld centerline. In the regions in which the peak temperature during welding remains lower than the austenite nucleation temperature during heating (A_{c_1}), no austenite is formed; instead, the originally retained austenite in the base metal may decompose. Therefore, to study the effect of such thermal cycles on the stability of retained austenite, a heat-treated base metal (condition HT840/400) sample was heated to 600 °C and cooled to room temperature at 0.03 °C s^{-1}. This heating ensures that the alloying element content of the phases remains the same and that the austenite present in the sample decomposes into ferrite and cementite. The saturation magnetization during heating ($M_{1H}(T)$) was measured as a function of temperature (T) by applying a constant field of 1 T (Figure 10). During this treatment, it can be expected that the austenite present in the samples transformed into ferrite and cementite. After cooling, this sample was again heated to 600 °C at the same heating rate (0.03 °C s^{-1}), and the saturation magnetization without austenite ($M_{2H}(T)$) was measured at the same temperatures (T). The difference between $M_{1H}(T)$ and $M_{2H}(T)$ yielded the decomposition behavior of austenite during heating.

The temperature-dependent saturation magnetizations of the samples with and without austenite ($M_{1H}(T)$ and $M_{2H}(T)$, respectively) were fitted with the well-known thermomagnetic equation:[11–13]

$$M(T) = M_o[1 - k(T + 273)^{3/2}] \qquad [3]$$

where k is a constant that, after the fitting, was found to be 1.1×10^{-5} K$^{-3/2}$ for $M_{1H}(T)$ and 1.5×10^{-5} K$^{-3/2}$ for $M_{2H}(T)$. M_o is the saturation magnetization at –273 °C and was found to be 165.8 Am^2/kg for the base metal sample with austenite (before first heating) and 192.1 Am^2/kg for the base metal sample without austenite (after first heating).

Figure 10(a) shows the variation in the saturation magnetization ($M_{1H}(T)$ and $M_{2H}(T)$) of the base metal sample (condition HT840/400) with respect to the temperature of heating. The $M_{1H}(T)$ initially starts reducing with an increase in the temperature due to the increase in spin-wave fluctuations. Once the temperature reaches 295 °C, $M_{1H}(T)$ gradually starts increasing due to the formation of ferromagnetic hcp ε carbide ($Fe_{2.4}C$) from the paramagnetic austenite. Upon further heating, there is an obvious decrease in the saturation magnetization in the temperature range 390 °C to 400 °C, which

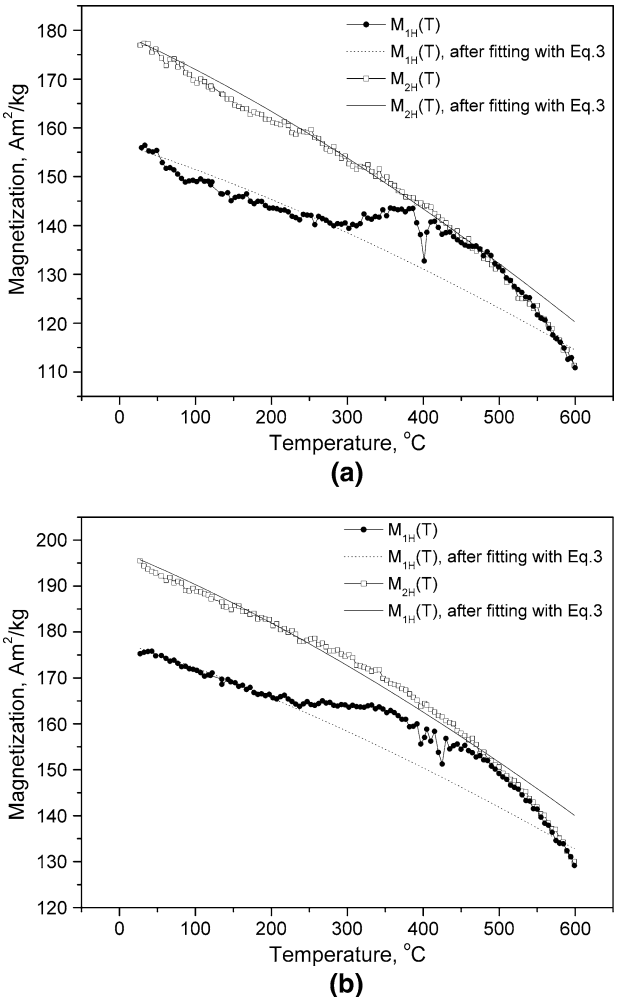

Fig. 10—Saturation magnetization as a function of temperature: (*a*) base metal sample and (*b*) fusion zone sample ($M_{1H}(T)$ is saturation magnetization of sample with austenite and $M_{2H}(T)$ is saturation magnetization of sample without austenite). Saturation magnetization values (M_s) were measured from these curves with an accuracy of ±0.01 Am^2/kg.

may be due to the formation of a paramagnetic transient phase. Further increase in the temperature results in the formation of stable cementite, which is paramagnetic above 210 °C, and the saturation magnetization decreases continuously until the final measurement temperature (600 °C). However, in the case of the second heating, the saturation magnetization $M_{2H}(T)$ decreases continuously with increasing temperature following Eq. [3], which indicates that there are no further transformations.

Thermomagnetic measurements were also carried out on a sample from the fusion zone of a welded TRIP steel in order to compare the decomposition behavior of austenite in the fusion zone to that of the base metal (Figure 10(b)). After fitting temperature-dependent saturation magnetizations of the fusion zone sample with Eq. [3], the constant k is found to be 1.2×10^{-5} for both $M_{1H}(T)$ and $M_{2H}(T)$. The saturation magnetization at –273 °C (M_o) was found to be 187.5 Am^2/kg for the fusion zone sample with austenite (before the first heating) and 209.8 Am^2/kg for the fusion zone sample without austenite (after the first heating). Table IV summaries the thermomagnetic parameters determined for the base metal and fusion zone samples. The calculated saturation magnetizations at –273 °C (M_o) were found be to higher than those for the base metal samples, while the magnetization behavior of the fusion zone sample appears to be similar to that of the base metal sample. However, the gradual increase in the magnetization, which indicates the formation of ε carbide ($Fe_{2.4}C$), is found at 240 °C, which is lower than for the base metal (290 °C). Moreover, the sudden decrease in the magnetization, which was found in the base metal sample, appears to occur over a slightly wider range of temperatures (370 °C to 410 °C), and the decrease in saturation magnetization occurs to a lesser degree in this temperature range.

Table IV. Measured Thermomagnetic Parameters for Base Metal and Fusion Zone Samples

First Heating ($1H(T)$)		Second Heating ($2H(T)$)	
k ($K^{-3/2}$)	M_o (Am^2/kg)	k ($K^{-3/2}$)	M_o (Am^2/kg)
Base Metal			
1.1×10^{-5}	165.8	1.5×10^{-5}	192.1
Fusion Zone			
1.2×10^{-5}	187.5	1.2×10^{-5}	209.8

IV. DISCUSSION

A. *Characteristics of Base Metals after TRIP Heat Treatment*

The cycles of the four different TRIP heat treatments (Figure 1) generated base microstructures with austenite contents varying from 3.6 to 14.0 pct. For the conditions HT840/400 and HT800/400, in which the isothermal bainitic holding temperature was 400 °C, a higher amount of retained austenite was obtained (8.9 and 14.0 pct, respectively), while samples held at 335 °C for IBT (conditions HT840/335 and HT800/335), the austenite content was found be 3.6 and 4.3 pct, respectively. Similar behavior was also observed by Saleh *et al.* in which lower bainitic holding temperatures resulted in lesser austenite fractions in the microstructures.[14] During isothermal bainitic holding, the austenite formed after the intercritical annealing transforms to carbide-free bainite, and the transformation ceases incompletely once the untransformed austenite is sufficiently enriched in carbon. The incomplete bainitic transformation time increases with decreasing isothermal bainitic holding temperature.[15] Minote *et al.* showed that for a 0.2 wt pct carbon TRIP steel, the incomplete bainitic transformation time varied from 80 to 1000 seconds when the isothermal bainitic holding temperature was reduced from 450 °C to 300 °C.[16] During the base metal heat treatments, IBT was carried out by holding at 400 °C and 335 °C for 60 seconds. This holding time was not sufficient to enrich the austenite and, especially in the cases of HT840/335 and HT800/335, there was

not enough time for the enrichment of carbon in austenite, in contrast to the samples held at 400 °C. As a result, the untransformed austenite after isothermal bainitic holding decomposes during subsequent cooling to room temperature and results in lesser austenite contents in HT840/335 and HT800/335 samples. Although the differences in the volume fraction of austenite between the base metal samples with higher (400 °C) and lower (335 °C) bainitic holding temperatures indirectly indicate insufficient enrichment of carbon at the lower bainitic holding temperature (335 °C), this cannot be confirmed directly because it is not possible to determine the carbon concentration from the magnetization measurements. Optical microscopy analysis also shows the presence of bulky austenite grains (approximately 5 μm in diameter) in the higher austenite-containing base metals (conditions HT840/400 and HT800/400), which indicates that more of the austenite grains, formed during intercritical annealing, remain untransformed during isothermal bainitic holding.

B. *Characteristics of Welded TRIP Steel Plates*

Magnetic saturation measurements show that significant amounts of austenite have been retained in the heat-affected and fusion zones of TRIP steel welds. It is interesting to note that the austenite contents in the center of the fusion zones were found to vary from 5.7 to 9.7 pct, despite the use of similar welding parameters. This is due to the partitioning of alloying elements during solidification and local variations in compositions due to the formation of nonmetallic inclusions, which in turn affect the stabilization of austenite, ultimately leading to variation in the austenite contents in the fusion zones. A previous study of the microstructural evolution during GTA welding of the steel under investigation confirms the partitioning of aluminum to the solidified δ ferrite and the formation of nonmetallic complex oxide-sulfite inclusions, which cause local variations in compositions in the fusion zone and thereby affect the stabilization of austenite.[2,17] The average amount of nonmetallic inclusions present in the fusion zones was 2.6 pct.

It is interesting to note that in the case of the base metal conditions HT840/400 and HT800/400, in which the starting austenite contents were higher (8.9 and 14.0 pct, respectively), the heat-affected zones were found to contain less austenite than the base metals. On the other hand, after starting from microstructures containing lesser austenite, as in the conditions HT840/335 and HT800/335 (3.6 and 4.3 pct respectively), the austenite contents increased in the heat-affected zones after welding (Figure 7). In the weld microstructures, the coarse and fine-grained heat-affected zones were found from 2.5 to 4.5 mm respectively, from the weld centerlines. A major portion of these zones, subjected to temperature ranges varying from 980 °C to 650 °C, with heating rates close to 500 °C/s, does not reach the intercritical $\alpha + \gamma$ region. In the case of the base metal conditions HT840/400 and HT800/400, the austenite grain sizes were found to be higher (approximately 5 μm) compared to the base metal conditions HT840/335 and HT800/335, and the higher isothermal holding temperature (400 °C) also resulted in lesser enrichment in carbon. As a result, the chemical stability and the stability due to the size of austenite in conditions HT840/400 and HT800/400 is lowered and the austenite in these samples decomposes more during heating compared to the austenite formed in HT840/335 and HT800/335.[18] Hence, it appears that during welding, less stable austenite in the base metals decomposes and new austenite grains nucleate above the A_{c1} temperature. These grains are retained at room temperature upon cooling after sufficient enrichment of carbon.

C. *Decomposition Behavior of Austenite*

The thermomagnetic measurements indicated that the austenite in the base metal started decomposing to ferromagnetic ferrite and ε carbides above 290 °C while heating at a rate of 0.03 °C s^{-1}. In the range 390 °C to 400 °C, there is a sudden decrease in saturation magnetization, which can be correlated to the formation of $\eta(\varepsilon')$ transient carbides. It is reported that at 400 °C, the orthorhombic $\eta(\varepsilon')$ transient carbide (Fe_2C) forms upon ordering from ε carbide by lowering the overall symmetry of the carbide phase on transforming from the hexagonal ε carbide to orthorhombic cementite (Fe_3C). In most of the cases occurring in the literature, it is observed in high-carbon steels,[19–21] with the exception of the observations by Jha *et al.*,[9] in which the formation of $\eta(\varepsilon')$ carbides was observed during the tempering of low-carbon steels containing austenite. However, the magnetic properties of this $\eta(\varepsilon')$-transient carbide are not reported anywhere due to the low stability of these carbides. It appears from the present observation that this transient $\eta(\varepsilon')$ carbide is paramagnetic, as observed in the temperature range 390 °C to 400 °C.

The thermomagnetic measurements on the fusion zone sample showed that the decomposition of austenite to ferrite and ε carbide ($Fe_{2.4}C$) started at 240 °C with a gradual increase in saturation magnetization. This is slightly lower than that of the base metal, which showed an increase in magnetization only above 290 °C. The difference may be attributed to the continuous cooling of the liquid weld metal to room temperature. Any austenite left in the fusion zone would be enriched in carbon compared with the base metal sample, which was held at 400 °C for the isothermal bainitic holding. This results in an earlier precipitation of ε carbide from the enriched austenite in the fusion zone sample compared to the base metal sample. The increase in the saturation magnetization in the fusion zone sample also occurs over a wider temperature range, from 240 °C to 460 °C, compared with the base metal samples. The base metal samples showed a narrow increased magnetization zone from 290 °C to 440 °C, despite the fusion zone sample containing less austenite (5.7 pct), compared with the base metal (8.9 pct). This indicates that the decomposition kinetics of austenite in the fusion zone sample is slower due to its size and carbon enrichment. The appearance of several sudden decreases in the magnetization indicates that the formation and decomposition of $\eta(\varepsilon')$-transient carbides may occur in several stages.

V. CONCLUSIONS

A quantitative analysis of the microstructural constituents in welded TRIP steels was carried out using magnetic saturation measurements. Approximately 4.1 to 12.6 pct austenite is found in the heat-affected zones and 5.7 to 9.6 pct is found in the fusion zones after welding, depending on the thermal history of the samples. The mass fraction of austenite present in the heat-affected and fusion zones reduces after welding the base metals containing a higher fraction of austenite. On the other hand, after starting from microstructures containing less austenite, the austenite contents increased in the heat-affected and fusion zones after welding. This is due to the presence of coarse and less stable austenite grains in the base metals with higher austenite contents. Thermomagnetic measurements showed that the decomposition kinetics of austenite in the fusion zone is slower than in the base metal. This measurement also indicated the formation of a paramagnetic orthorhombic $\eta(\varepsilon')$-transient carbide (Fe_2C) during the decomposition of austenite. While it is possible to explain the experimental observations in terms of the formation of transient $\eta(\varepsilon')$ carbides, further experimental evidence should be sought to consolidate this finding.

ACKNOWLEDGMENTS

This research was carried out under Project No. MC8.04188 in the framework of the Research Program of the Materials Innovation Institute M2i (www.m2i.nl), the former Netherlands Institute for Metals Research. The authors gratefully acknowledge the welding research group, Research and Development, Corus (IJmuiden, The Netherlands), for their interest in this project.

OPEN ACCESS

REFERENCES

1. B.C. De Cooman: *Curr. Opin. Solid State Mater. Sci.*, 2004, vol. 8, pp. 285–303.
2. M. Amirthalingam, M. Hermans, and I. Richardson: *Metall. Mater. Trans. A*, 2009, vol. 40A, pp. 901–09.
3. N. Kapustika, C. Conrardy, S. Babu, and C. Albright: *Weld. J.*, 2008, vol. 87, pp. 135s–148s.
4. L. Zhao, N.H. van Dijk, E. Bruck, J. Sietsma, and S. van der Zwaag: *Mater. Sci. Eng., A*, 2001, vol. A313, pp. 145–52.
5. B.D. Cullity: *Introduction to Magnetic Materials*, Addison-Wesley, Reading, MA, 1972.
6. E. Girault, P. Jacques, Ph. Harlet, K. Mols, J. Van Humbeeck, E. Aernoudt, and F. Delannay: *Mater. Charact.*, 1998, vol. 40, pp. 111–18.
7. L. Zhao, M.K. Wibowo, M.J.M. Hermans, S.M.C. van Bohemen, and J. Sietsma: *J. Mater. Process. Technol.*, 2009, vol. 209, pp. 5286–92.
8. N. Luzginova, L. Zhao, and J. Sietsma: *Mater. Sci. Eng., A*, 2007, vol. A448, pp. 104–10.
9. B.K. Jha and N.S. Mishra: *Mater. Sci. Eng., A*, 1999, vol. A263, pp. 42–55.
10. H. Yin: *Iron Steel Technol.*, 2006, June, pp. 64–73.
11. L. Zhao, F.J. Vermolen, J. Sietsma, and S. van der Zwaag: *J. Mater. Sci. Technol.*, 2003, vol. 19, pp. 105–08.
12. A.S. Arrott and B. Heinrich: *J. Appl. Phys.*, 1981, vol. 53 (3), pp. 2113–15.
13. C. Kittle: *Introduction to Solid State Physics*, 6th ed., John Wiley & Sons Inc, New York, NY, 1986, p. 429.
14. M.H. Saleh and R. Priestner: *J. Mater. Process. Technol.*, 2001, vol. 113, pp. 587–93.
15. E. Girault, P. Jacques, P. Ratchev, J. Van Humbeeck, B. Verlinden, and E. Aernoudt: *Mater. Sci. Eng., A*, 1999, vols. A273–A275, pp. 471–74.
16. T. Minote, S. Torizuka, A. Ogawa, and N. Nikura: *ISIJ Int.*, 1996, vol. 36 (2), pp. 201–07.
17. M. Amirthalingam, M.J.M. Hermans, and I.M. Richardson: IIW Document Nos. IX-2291-08 and IX-L-1029-08, International Institute of Welding, 2008.
18. J. Wang and S. van der Zwaag: *Metall. Mater. Trans. A*, 2001, vol. 32A, pp. 1527–39.
19. Y. Hirotsu and S. Nagakura: *Acta Metall.*, 1972, vol. 20, pp. 645–55.
20. Y. Hirotsu, Y. Itakura, K. Su, and S. Nagakura: *Trans. JIM*, 1976, vol. 17, pp. 503–13.
21. J.H. Jack: *J. Iron Steel Inst.*, 1951, vol. 169, pp. 26–36.